Save time. Save sample. Save effort. Save money.

Get all the advantages of high-parameter flow cytometry packaged in an easy-to-use and highly economical format with the new CyTOF XT.™

CyTOF technology provides

- Maxpar® Direct™ Assays: easy, efficient, high-parameter immune-profiling kits with a software solution
- the most data for every cell: 50-plus unique markers per panel
- flexible workflows: stain, freeze, store and ship samples

CyTOF XT is

- fully automated: hands-free instrument calibration, sample resuspension and acquisition
- easy to use: simplified cleaning and maintenance workflows
- highly economical: automation frees lab personnel, lower price point frees budget

STANDARD BIOTOOLS™
Formerly Fluidigm

Hear how CyTOF XT is advancing precision medicine.

CyTOF® XT

Cytometry 6:81–91 (1985)

A Comparison of Different Focus Functions for Use in Autofocus Algorithms

Frans C.A. Groen, Ian T. Young, and Guido Ligthart

Department of Applied Physics, Delft University of Technology, 2600 GA Delft, The Netherlands

Received for publication March 6, 1984; accepted October 16, 1984

A number of functions for the autofocusing of microscopes and other optical instruments are to be found in the literature. In this article we compare 11 of them to determine, in an objective manner, which functions are most suitable for implementation with real-time video acquisition systems. Three different images, each representing a typical class of image, are used in the comparison. Among the best focus functions found in our study are the squared magnitude gradient, the squared Laplacian, and the normalized image standard deviation.

Key terms: Focus function, image focus, comparative study, gradient, Laplacian

Autofocus algorithms are of particular importance in scanning microscope systems. The focus may have to be adjusted when the system mechanically moves from field to field, or when there is mechanical drift between two scans of the same field. In general algorithms that determine optimal focus for an image are based upon maximizing or minimizing some function that represents a "figure-of-merit." Algorithms have to be fast, as the total scan time is usually important. Thus the focus criterion functions used in the algorithms must be easy to calculate as, for example, with hardware and the video signal from a TV camera.

A number of focus functions have been proposed in the literature. Some of these deal only with special applications, while others are more generally applicable. The purpose of this study is to compare different proposed focus functions and determine their domain of general or special applicability. A literature search was conducted for focus functions which could be derived from the video signal. Such functions are at an extremum when the system is in focus. A general model for such a function is given in Figure 1 as well as some definitions of properties of the function.

The following criteria are used in the selection and evaluation of the focus functions:

a) *Unimodality.* The focus function must be unimodal; i.e., only a single maximum or minimum should be present. This simplifies considerably an autofocus algorithm and avoids potential errors from local extrema.

b) *Accuracy.* The extremum must be present when the system is in focus.

c) *Reproducibility.* A sharp top of the extremum results in good reproducibility.

d) *Range.* The range over which an in-focus image can be attained must be as large as possible. This means that the extremum must be broadly tailed.

e) *General applicability.* The focus functions must not be limited to some special type(s) of images.

f) *Insensitivity to other parameters.* If during the focus process other parameters change (e.g., mean brightness of the image), the autofocus process should not be disturbed.

g) *Video signal compatibility.* It is usually desirable for the focus function to be based on the same video signal that is used as input for image analysis. In this way a systematic focus error, which is the result of a positioning error between the focus detectors and the image scanning system, can be avoided.

h) *Implementation.* The system must be easy to implement.

In the next sections 11 different focus functions are described. Results with the functions applied to three different images are given, and finally some concluding remarks are made.

CLASSES OF FOCUS FUNCTIONS

The defocussing of an optical system can be modelled, to a first approximation, by the convolution of the image with a certain class of point-spread functions.

In the spatial frequency (Fourier) domain this convolution is equivalent to the multiplication of the image frequency spectrum with an optical transfer function. Optical transfer functions of focussed and defocussed systems are discussed by Goodman (5) and Hopkins (6), and a typical example is shown in Figure 2. When an optical system is defocussed, the high spatial frequency content of the resulting image decreases. Thus a focus function can be obtained from some measure of the high

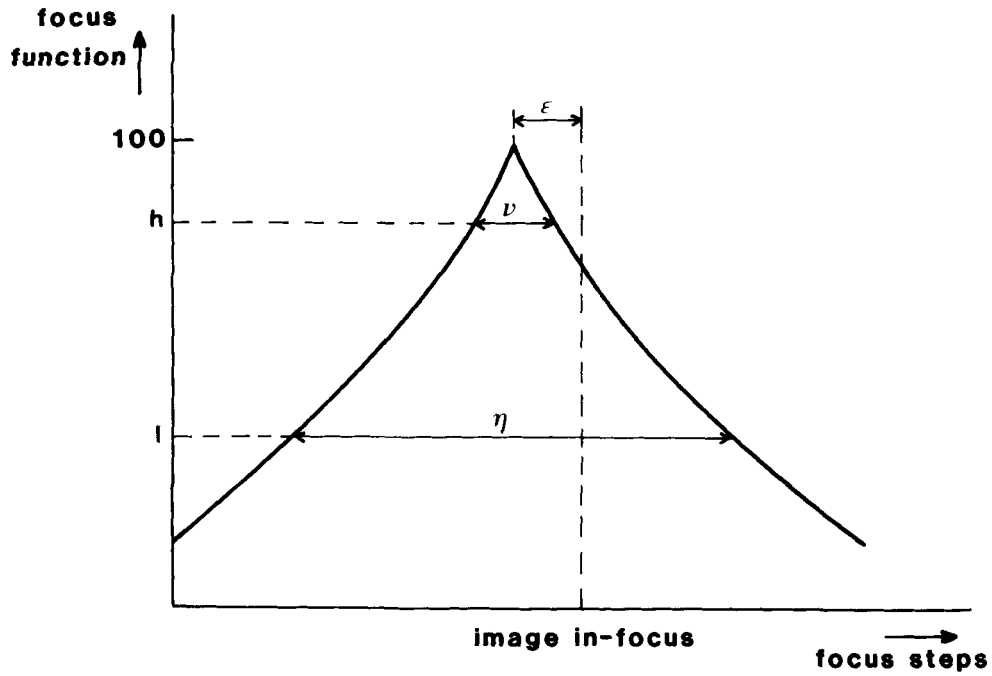

FIG. 1. Focus function: ϵ is the difference (in focus steps) between the in-focus image and the extremum, ν is the width at a high percentage of the maximum, η is the width at a low percentage of the maximum. For an ideal focus function $\epsilon = 0$ (no systematic errors), ν is small (reproducible) and η is large (wide focus range).

frequency content in the output image. As a result of the decrease in high frequencies in the output image, sharp edges become faint, and small dark or bright objects in the image become less dark or bright. Again this is due to the spreading caused by the point-spread function and the fact that energy is conserved in the (assumed) lossless transfer function. By measuring the contrast (or height) of the resulting grey-value peaks, focus functions can also be obtained.

Based upon the changes that occur in high frequency content as well as the changes that occur in the edges of pictorial objects, the investigated focus functions fall into three general categories:

$$1)\ F^1_{n,m,\Theta} = \iint_{\text{image}} E\left\{\left|\frac{\partial^n g(x,y)}{\partial x^n}\right| - \Theta\right\}^m dxdy \quad (1)$$

in which g (x,y) is the grey value at (x,y), Θ is an arbitrary threshold and $E(z) = z$ if $z \geqslant 0$; $E(z) = 0$ if $z < 0$. In this first function (F^1) the higher-frequency components in the image are measured by differentiation of the image and summing the values over the image.

$$2)\ F^2_{f,\Theta} = \iint_{\text{image}} f[g(x,y) - \Theta]\, dxdy \quad (2)$$

in which f(z) is a function chosen to measure the depth or size of peaks or valleys within the image.

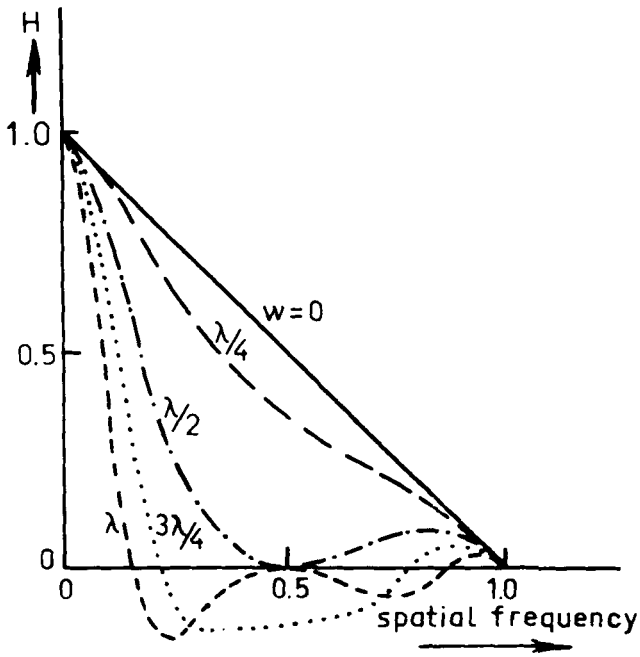

FIG. 2. Optical transfer function (H) of an in-focus (w = 0) and defocussed system (w ≠ 0) with square aperture and incoherent illumination.

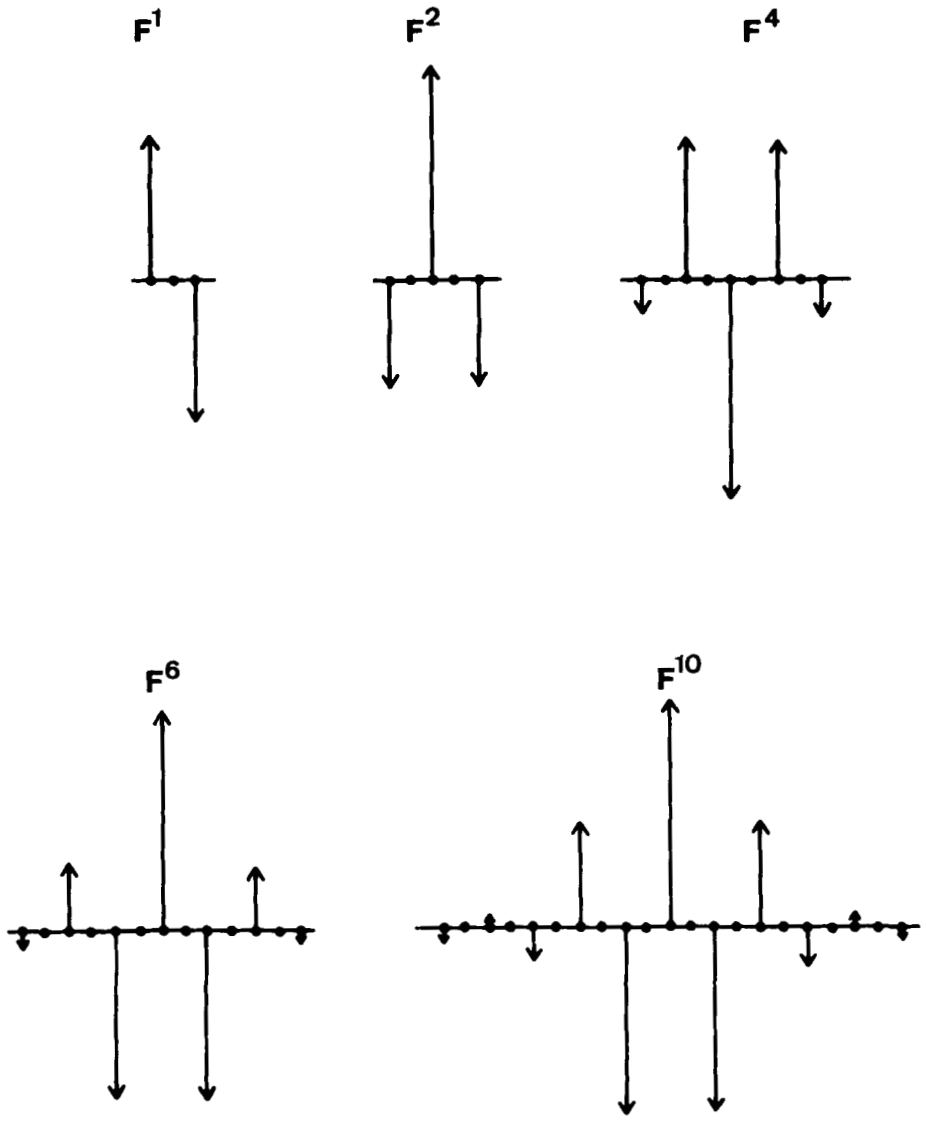

FIG. 3. Filter functions in the spatial domain corresponding to $F^n(\Omega)$ (Eq. 5) (according to Linge).

$$3)\ F^3_{m,c} = \frac{1}{c} \iint_{image} | g(x,y) - \bar{g} |^m \, dxdy \qquad (3)$$

in which c is a normalizing constant and $\bar{g}$ is the mean grey-value over the image. In this function the contrast or the variance in the image may be measured.

Focus Function Based on Differentiation: $F^1_{n,m,\Theta}$

An important issue is how the derivatives of the image are measured. When the image is digitized, an approximation can be obtained by a first- or second-order difference, such as:

$$\frac{\partial g(x,y)}{\partial x} \simeq \frac{\Delta g}{\Delta x} = g(i,j) - g(i,j-1) \qquad (4a)$$

$$\frac{\partial^2 g(x,y)}{\partial x^2} \simeq \frac{\Delta^2 g}{\Delta x^2} = g(i,j+1) - 2g(i,j) + g(i,j-1) \qquad (4b)$$

Better estimates for the first- and higher-order derivatives are proposed by Linge et al. (10) and are based on

filters of which the discrete Fourier transforms $F(\Omega)$ are given by

$$F^n(\Omega) = [\sin(\pi\Omega/\Omega_N)]^n \quad (5)$$

in which Ω_N is the Nyquist frequency and Ω is the spatial frequency. In Figure 3 some of these filters in the spatial domain are shown.

Compared to the first- and second-order differences (Eqs. 4a, 4b, resp.), $F(\Omega)$ gives a better noise reduction at the highest spatial frequencies because this filter selects a band out of the total spectrum and yet still has a differentiating character within the selected band. For each function a–d below, calculation with Equations 4 and 5 will be compared.

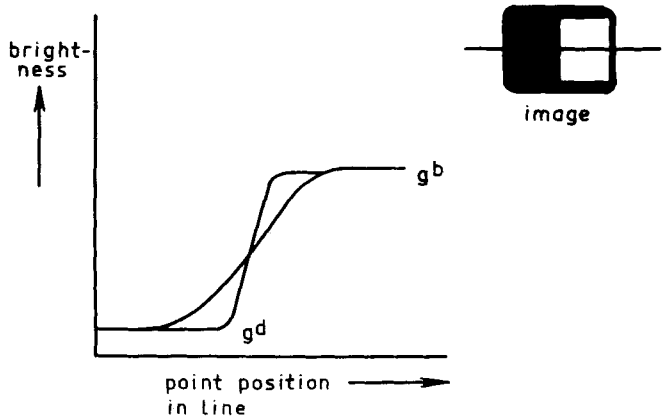

FIG. 4. For large objects the sum of the absolute differences will always be the difference over the edge: $g_b - g_d$, whether the image is in focus or not.

Absolute gradient. This function was proposed by Jarvis (7) and is obtained by setting n = 1, m = 1, $\Theta = 0$ in F^1: so $f_a = F^1_{1,1,0}$. For objects which are small compared to the size of the point-spread function, this function works well. This can be explained by noting that the heights of the grey-value peaks decrease when the image is defocussed. When objects are present that are large compared to the size of the point-spread function, only the slope of the edge is changed by defocussing. Particularly when $\partial g/\partial x$ is calculated by the first difference, the sum of the absolute differences will always be the total difference in brightness over the edge, as long as the point-spread function is small compared to the object size. This is illustrated in Figure 4.

Thresholded absolute gradient. This function is a variant of the previous one. By only summing those differences larger than a certain threshold, only the larger gradients, which are representative of the focussed situation, are taken into account. In F^1 $\Theta \neq 0$:$f_b = F^1_{1,1,0}$.

Squared gradient. This function is described by Muller and Buffington (13) and Erteza (3,4). By squaring, the algorithm enhances the larger gradients over the smaller ones. It responds to the steepness of an edge and hence does not degenerate for large objects. It therefore responds to objects more equally, regardless of size compared to pixel spacing. The advantage of this function

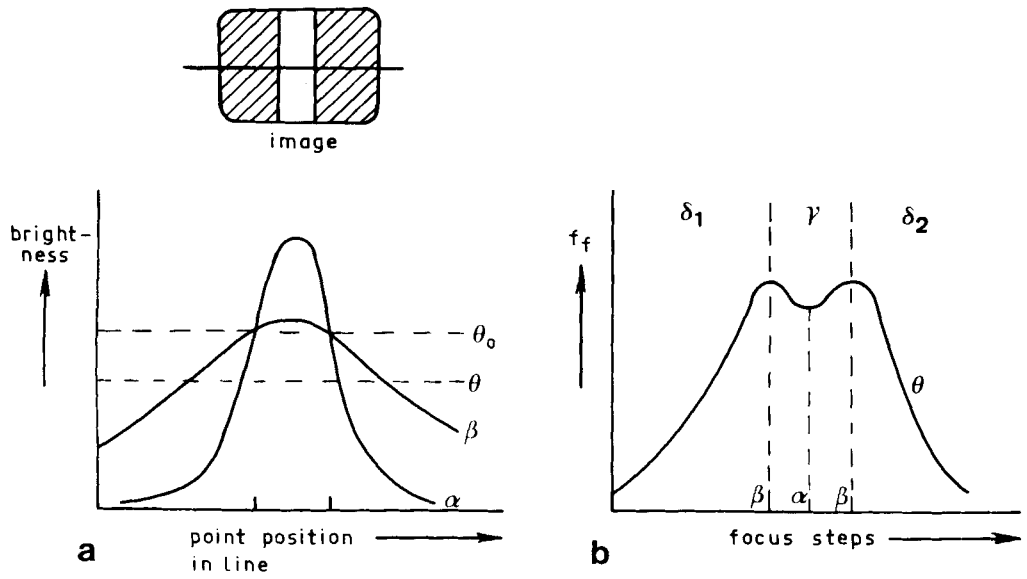

FIG. 5. Focus function for an image containing a bright strip. When the threshold is smaller than Θ_0 the pixel count (peak width in a) in the focussed situation (α) will be smaller than when it is slightly defocussed (β). This results in b) an increase in the function f_f from the in-focus situation.

over the thresholded absolute gradient is that it has no threshold to adjust and yet is still based upon the same principle. In $F^1\ \Theta = 0$, m = 2, n = 1: $f_c = F^1_{1,2,0}$.

Laplacian. The sum over the image of the squared second derivatives is used by Muller and Buffington (13) and by Erteza: in $F^1\ \Theta = 0$, m = 2, n = 2 : $f_d = F^1_{2,2,0}$.

In the Fourier domain, the transfer function of a second-order difference filter (Laplacian) enhances the higher spatial frequencies more strongly than the first-order difference filter (gradient).

According to Erteza (3,4) the second-order difference should be better suited than the first-order difference, as the width of the top of the extremum of the focus function is smaller. Erteza found also that the second-order function gave better results than third or higher orders, because of the increase in noise effects in these filters.

Focus Functions Based on Depth of Peaks and Valleys: $F^2_{f,0}$

Thresholded video-signal content. This function is the summation of that portion of a video signal that is above (or below) a threshold. This function was described by Mendelsohn and Mayall (12) and further investigated by Mason and Green (11) and Johnson and Goforth (8).

In F^2 the function f(x) = E(x) (above the threshold) or f(x) = E(−x) (below the threshold), so

$$f_e = F^2_{f(x)\,=\,E(\pm x),\Theta}$$

This algorithm was originally designed and tested on metaphase images of chromosomes. The position of the extremum (in-focus) proved, according to the researchers, to be independent of the chosen threshold (except for very large thresholds, where focussing is not possible). The shape of the extremum of the focus function is dependent on the threshold setting.

Thresholded video-signal pixel count. The function is the number of pixels in the image above or below a certain threshold. So in F^2 the function f(x) = s(x), in which s(x) = 1 if x > 0 or else s(x) = 0 or the complementary version:

$$f_f = F^2_{f(x)=s(-x),\Theta}$$

The algorithm is described by Van Daele et al. (2) and in a patent of Zeiss, GmbH (1).

Mendelsohn and Mayall (12) also mention this algorithm. They reject it because the extremum position depends on the chosen threshold (see also Fig. 5). In Figure 5a we see the video signal of a line of an image containing a bright slit in a dark background. In this figure α is a scanline from a better focussed image than β. When the threshold is higher than Θ_0, α contains more counted pixels than β, and when the threshold is lower than Θ_0, β contains more counted pixels than α. The result of this property is that the number of pixels f_f as a function of the focus distance looks like Figure 5b for thresholds $< \Theta_0$. By changing the threshold, the width of the region, γ, can be adjusted. The smaller the region γ is chosen, the smaller also the range δ is. There are two ways to use this function: (1) maximization in region δ (Van Daele) or minimization in region γ (Zeiss).

Signal power. The sum of the squared grey-values over the image is described by Muller and Buffington (13). In this case in F^2 the function $f(x) = x^2$ and $\Theta = 0$.

$$f_g = F^2_{f(x)\,=\,x2,0}$$

In addition to this function they describe seven other algorithms, which were disregarded in this study because they were very difficult to implement.

Focus Functions Based on the Image Contrast: $F^3_{m,c}$

Variance. The use of the variance of the grey-values in an image has been proposed by the Kernforschungs Zentrum Karlsruhe GmbH (9). Thus M = 2 and c = A $= \iint_{\text{image}} dxdy$: the image area.

$$f_h = F^3_{2,A}$$

In comparing this function to the function based upon signal power, we see that not only the large bright values (above the mean) contribute strongly to the function, but large black values (below the mean) as well.

Normalized variance. This function, the variance divided by the squared mean, a variant of the previous one, is also described in the Kernforschung Zentrum patent (9). The normalization of the variances compensates for changes in the average image brightness. Thus m = 2 and $c = A \cdot \bar{g}^2$.

$$f_i = F^3_{2,A\bar{g}^2}$$

Absolute variation. As the computation of the variance is rather complicated, a comparable result could be expected from the much easier to calculate absolute difference. Thus m = 1 and c = A, the image area:

$$f_j = F^3_{1,A}$$

Normalized absolute variation. In this variation the absolute difference with the mean is divided by the mean. Thus m = 1 and $c = A \cdot \bar{g}$.

$$f_k = F^3_{1,A\bar{g}}$$

EXPERIMENTS AND RESULTS

Three different images were used to investigate the various focussing algorithms. Each image was scanned a number of times (to be described later) at different focus positions of the scanning instrument. The three images are representative for a certain class of image types to which it was expected from the previous discus-

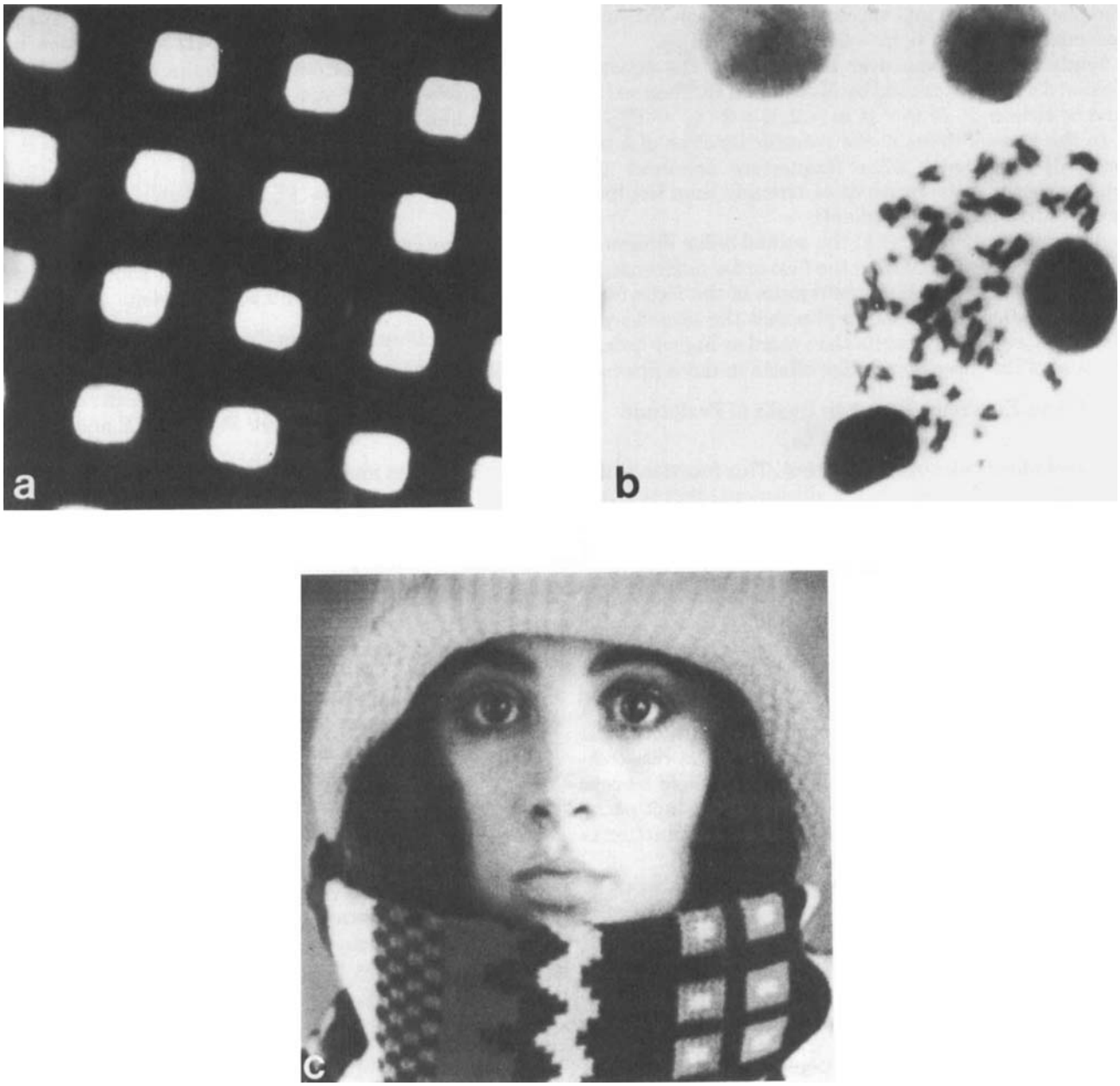

FIG. 6. Images used: a) *grid*, b) *metaphase*, c) *portrait*.

sion that the focus functions would respond very differently. The images used were the following:

1) *An electron microscope grid*: The image is shown in Figure 6a and is representative of images with large object and background portions, such as images with background and dirt. The multiple scans of the image were done with a light microscope and a 25× objective lens. The difference between two successive scans was a change in the focus step of 4 μm. Important features of this image are only high or low brightness, large objects of constant brightness, low mean brightness.

2) *A metaphase spread*: This image consists of a bright background with dark objects (chromosomes and cell nuclei) and is representative of images with a large number of objects. The test image used is given in Figure 6b. The images were scanned with a light microscope and a 100× oil-immersion objective. The difference

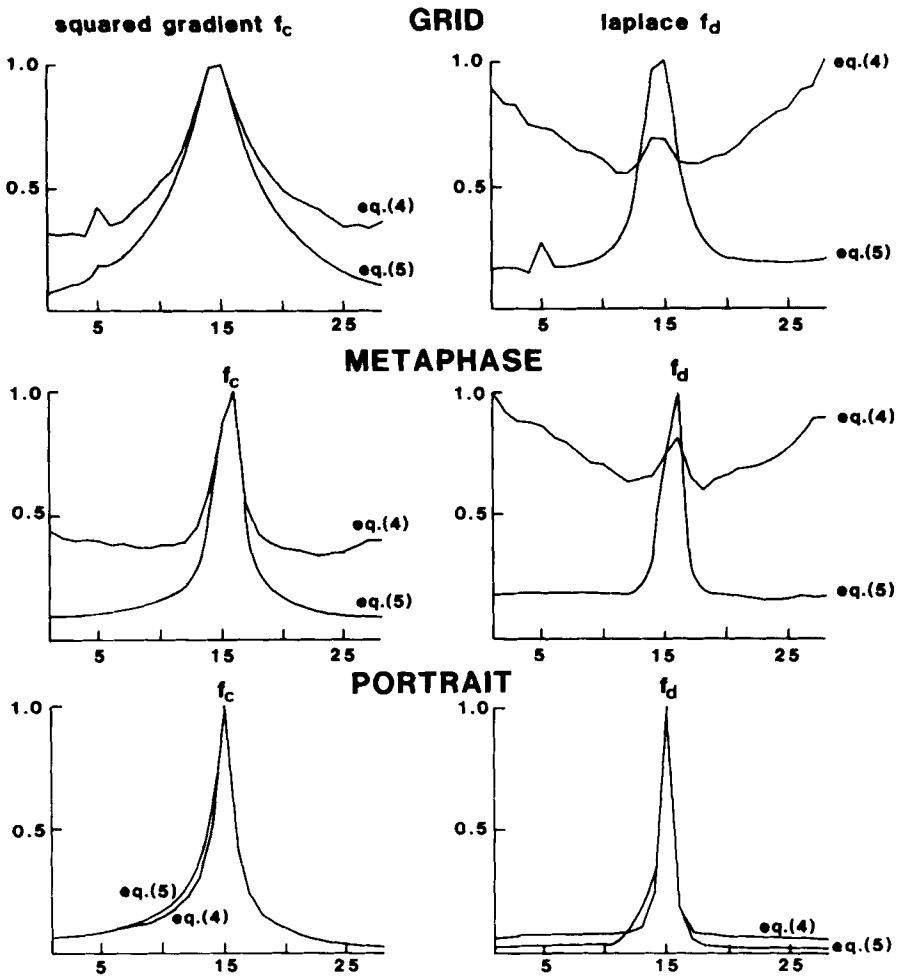

FIG. 7. Functions f_c (squared gradient) and f_d (Laplace) calculated according to Equation 4a (left) or 4b (right) and Equation 5 (n = 1, left or n = 2, right) for the three sequences.

between two successive focussing steps here is 1 μm. Features of these images are large bright background, small objects, high mean brightness.

3) *Portrait*: This macroscopic image, given in Figure 6c, was chosen because some focus functions were developed for this type of image with lots of fine detail. The image was scanned with a TV camera at full opening (lens: f 2.0/80). The in-focus distance between the lens and photograph was 520 mm. Focussing took place by moving the camera with respect to the object in 20-mm steps. In this image sequence a relatively large change in image content is present related to the relatively large depth of field of the macro setup. This poses a separate problem from the variation in fixed-content images. Features of the image are many different brightness values, many small structures, low mean brightness, varying image content in the focussing sequence.

Standard Deviation in the Function Values

Before beginning with the evaluation of different focussing algorithms it is first important to understand how much variation there is in the measured functions owing to noise and other sources. To assess this the standard deviation in the measured function values was investigated by scanning each image 10 times. The result was that the standard deviation in the function values was 1% of the maximum function value or less. A single exception was the Laplacian function f_d, where the standard deviation was 2%.

Only the reproducibility owing to repeated scanning was investigated. Reproducibility tests to assess the ef-

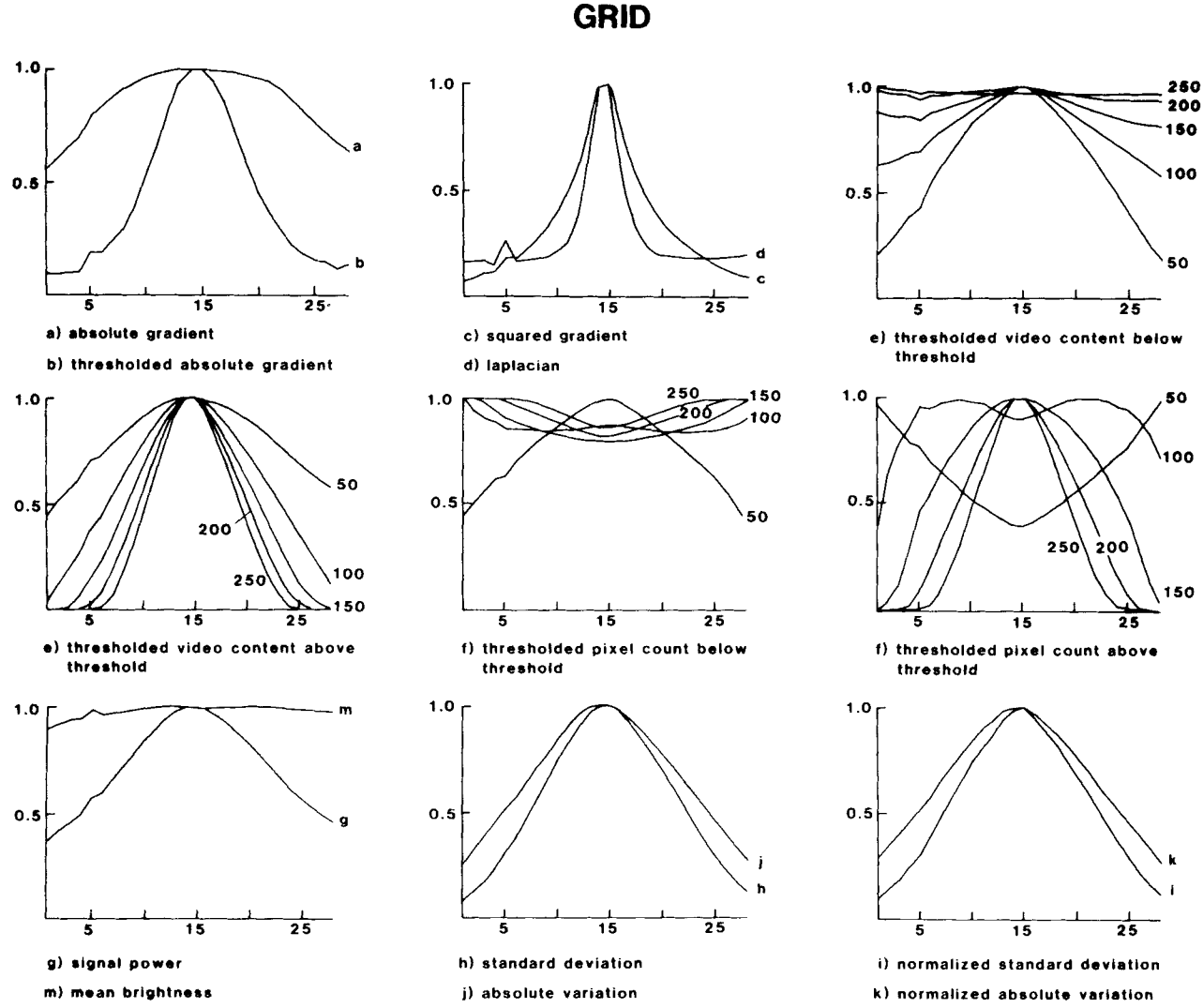

FIG. 8. Functions f_a–f_k and mean brightness for the *grid* sequence (f_a,f_c,f_d calculated with Eq. 5; f_h with Eq. 4).

fects of changing image coverage with focus and the influence of parameters such as mean brightness were not included in this experiment.

Comparison of the Focus Functions

For each image sequence 28 focus steps were made. Each situation represents the change from an out-of-focus image through an in-focus image and then continuing, once again, to an out-of-focus image. The image in the middle of the sequence is the visual in-focus image. The visual in-focus images were *grid*, 15; *metaphase*, 16; *portrait*, 15.

In Figure 7 the focus functions are given for different estimates of the derivative of an image. In figures 8–10 the functions for the three image sequences are given. Each function is normalized, so that its maximum is 1. In Table 1 the width of the extrema of the functions are given at 50% and the 80% width (sharpness of the top) as an indication of the reproducibility.

We first compare the focus functions that are based on differentiation. The influence of the different estimates of the derivatives is illustrated in Figure 7. For an image such as *portrait*, where many edges are present, the difference in the focus functions based on Equation 4 or 5 is small. For an image such as *grid*, where only a few edges are present, the estimates based on Equation 5 are considerably better, particularly the second-order derivative (Laplace). Estimates according to Equation 5

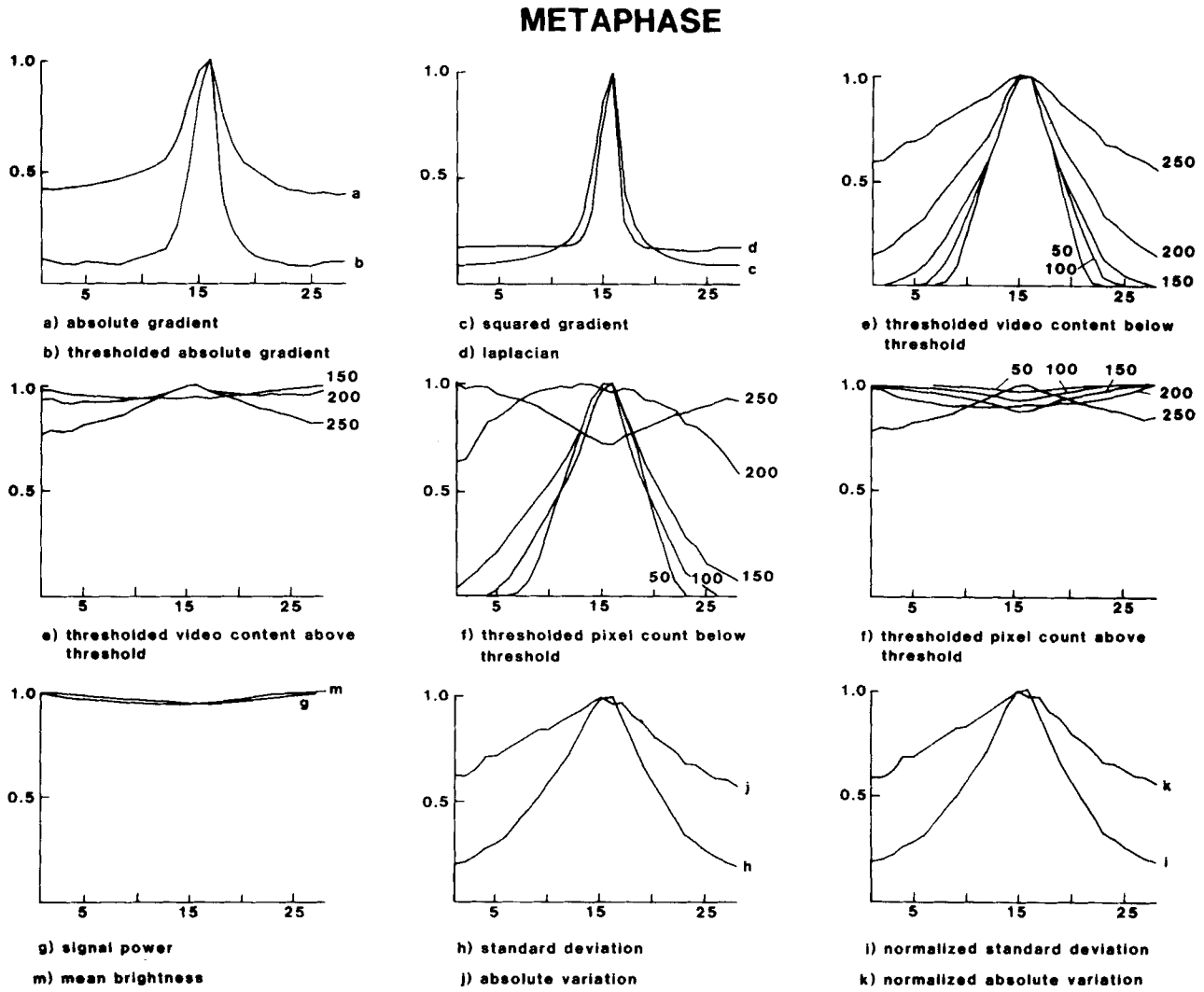

FIG. 9. Functions f_a–f_k and mean brightness for the *metaphase* sequence (f_a,f_c,f_d calculated with Eq. 5; f_b with Eq. 4).

and proposed by Linge et al. (10) are therefore preferable to the simplistic first and second differences.

The simplest function f_a (absolute gradient) is usable for *portrait* and *metaphase* but poor for *grid* (see Figs. 8–10). This last result can be explained by the fact that in *grid* the object sizes are large compared to the point-spread functions so the sum of the absolute gradient will be almost constant.

By taking only larger differences into account, as is done with f_b (thresholded absolute gradient), the function f_b (for both estimates) can be used for all three images. The only problem is that the choice of the threshold depends on the image for an optimal result.

The squared first derivative (f_c) and the squared second derivative (f_d) give a nice peak for all three images. Particularly for *portrait* and *metaphase*, a sharp extremum is present. The peak of f_d is smaller than f_c, as could be expected. When we investigate functions f_e and f_f (thresholded video content and thresholded pixel count), we see that the result is only good when the "sign" (summation above or below the threshold) is correctly chosen. For *metaphase* and *portrait*, summation has to be done below the threshold, for *grid* above the threshold. This choice depends upon whether many small dark or small bright picture parts are present in the image.

When the sign is correctly chosen, f_e and f_f give the best result for *metaphase* (for which they were originally designed) and the worst for *portrait*. The video content (f_e) is to be preferred over the pixel count (f_f), since, when

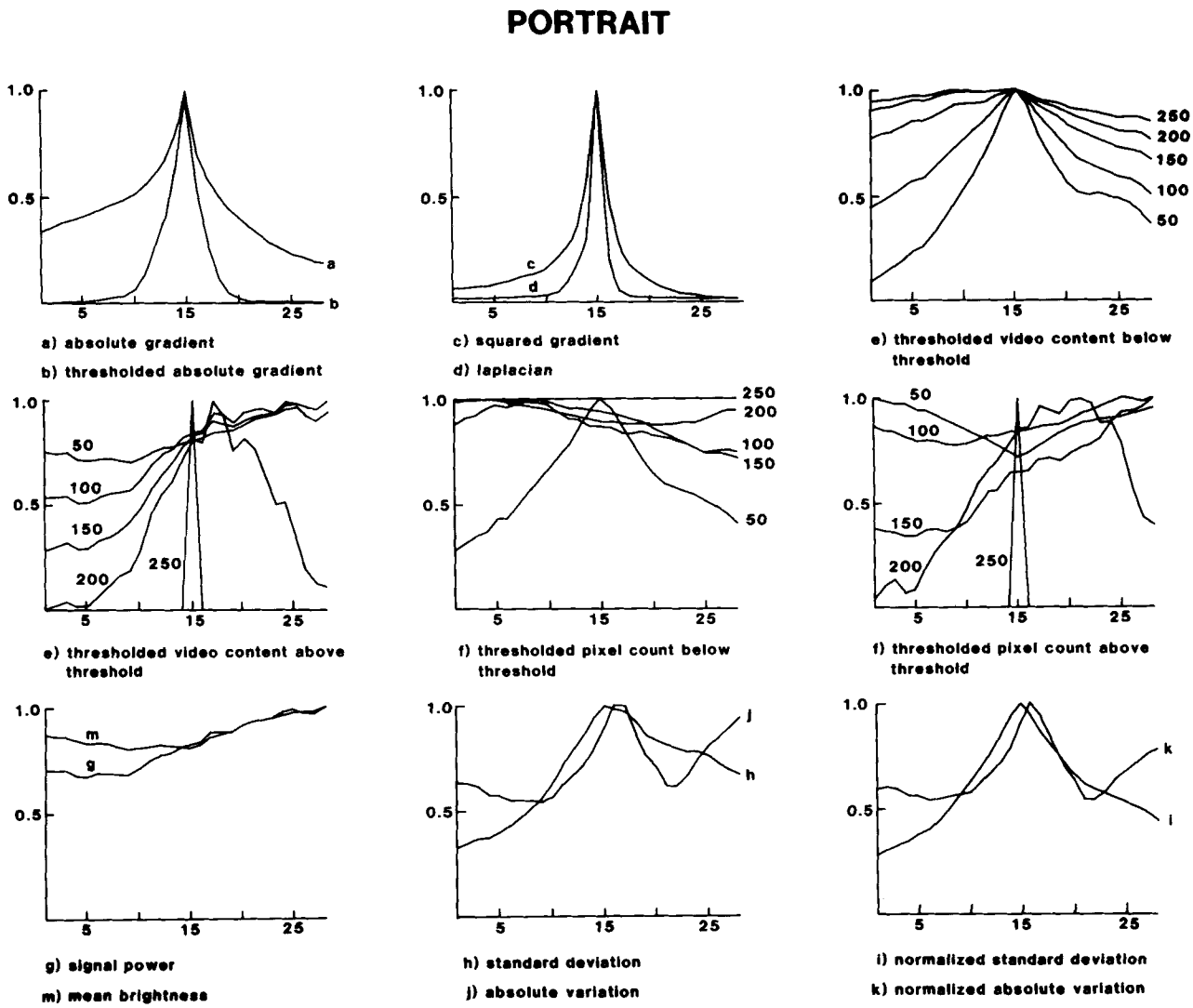

FIG. 10. Functions f_a–f_k and mean brightness for *portrait* sequence (f_a,f_c,f_d calcualted with Eq. 5; f_b with Eq. 4).

Table 1
Peak Width at 50% and 80% of the Maximum Value[a]

	Image sequence					
	Grid		Metaphase		Portrait	
Function	50% (μm)	80% (μm)	50% (μm)	80% (μm)	50% (mm)	80% (mm)
a	—	77	10.2	2.8	176	32
b(θ = 20)	40	23	2.7	1.4	56	16
c	30	12	3.2	1.6	48	18
d	16	8	2.5	1.0	26	12
e	36–112	20–60	8–28	4–12,5	252–500	80–160
f	36–76	20–46	8–11	3.5–4.5	36.8	11,6
g	91	44	—	—	—	—
h	61	32	12,5	5	—	196
i	61	39	12	5	372	112
j	87	90	—	13	—	—
k	89	40	—	12	—	—

[a]These are, respectively, indications for the range and the reproducibility.

the sign is correct, the threshold choice is not too critical. The main objection against these methods, however, remains the choice of the sign and the threshold value.

The function f_g (signal power) only gives a usable peak for *grid*, where the mean brightness is low and relatively stable. For *portrait* and *metaphase* this function cannot be used.

When we compare the functions based upon standard deviation (h,i) to the functions based upon absolute variation (j,k), we find that the simplification of taking the absolute value instead of squaring produces inferior results in terms of the shape of the functions and in the peak positions. We found this same result also in the comparison between the absolute gradient (a) and the squared gradient (b).

When we compare functions (h,j) with (i,k), we see that normalization of the function by division with the mean brightness only gives a significant improvement for *portrait*. Functions h and i are particularly usable as the peak tails are wide and thus the autofocus range will be large.

DISCUSSION

When we look at the results for the different images the results are as follows. *Grid*: The squared derivatives f_c–f_d and the standard deviation functions (f_h–f_k) give the best results. *Metaphase*: Besides the squared derivatives (f_c–f_d), the use of the video content below the threshold (f_e) and the pixel count (f_f) are very usable, although there is still the problem of threshold selection. In addition the standard deviation functions (f_h–f_k) give good results. *Portrait*: The squared first and second derivatives give very narrow peaks. The normalized standard deviation (f_i) can also be used.

Two functions are generally usable without the setting of thresholds: the squared derivatives f_c and f_d and the standard deviation divided by the mean f_i (where the division gives only a slight improvement).

Function i has wide tails of the extremum, giving a large autofocus range; functions c and d have narrow peaks, resulting in good reproducibility. For those images where f_i produces suboptimal results (as, for example, in *portrait*), f_c appears to produce extremely good results. A focus function based upon a combination of the two techniques—squared derivative and normalized variance—would provide a focussing algorithm with both wide focus range and good reproducibility.

While it is difficult to draw definitive conclusions from only three images, the results shown in Figures 8–10 indicate strongly that the focus functions based upon squared derivatives, f_c and f_d, and the standard deviation normalized by the mean, f_i, provide the desired properties for an automated focussing algorithm. We have implemented these functions in a microprocessor-controlled autofocus device and are in the process of testing its overall suitability.

LITERATURE CITED

1. Carl-Zeiss-Stiftung: Method of and device for the automatic focussing of microscopes, Patent specification 1314313, London, (1973).
2. Daele J van, Dom F, Buysscher L de, Oosterlinck A, Berghe H van den: Metaphase finding using microprocessors. IEEE Computer Society Conference on Pattern Recognition and Image Processing, August 6–8, Chicago (460–465), 1979.
3. Erteza A: Sharpness index and its application to focus control. Appl Opt 15:877, 1976.
4. Erteza A: Depth of convergence of a sharpness index autofocus system. Appl Opt 16:2273, 1977.
5. Goodman JW: Introduction to Fourier Optics. McGraw-Hill, New York, 1968.
6. Hopins HH: The frequency response of a defocused optical system. Proc Roy Soc A 231:91–103, 1955.
7. Jarvis RA: Focus optimisation criteria for computer image processing. Microscope 24:163, 1976.
8. Johnson ET, Goforth LJ: Metaphase spread detection and focus using closed circuit television. J Histochem Cytochem 22:563, 1974.
9. Kernforschungszentrum Karlsruhe GMBH: Verfahren und Einrichtung zur automatischen Scharfeinstellung eines jeden Bildpunktes eines Bildes. Patent specification PLA 7907 Karlsruhe, 1979.
10. Linge H, Zimmer HG, Neuhoff V: Focus adjustment in linear systems. Proceedings ISMIII, Berlin, Oct. 26–28, 1982, pp 40–45.
11. Mason DC, Green DK: Automatic focussing of a computer-controlled microscope. IEEE Trans Biomed Engineer 22:312, 1975.
12. Mendelsohn ML, Mayall BH: Computer-oriented analysis of human chromosomes-III focus. Comput Biol Med 2:137, 1972.
13. Muller RA, Buffington A: Real-time correction of atmospherically degraded telescope images through image sharpening. J Opt Soc Am 64:1200, 1974.